Gravitational wave nonlinearities and pulsar-timing array angular correlations

Gianmassimo Tasinato

Physics Department, Swansea University, Swansea SA28PP, United Kingdom

(Received 11 February 2022; accepted 24 March 2022; published 11 April 2022)

Several pulsar-timing array (PTA) collaborations are finding tantalizing hints for a stochastic gravitational wave background signal in the nano-Hertz regime. So far, though, no convincing evidence for the expected Hellings-Downs quadrupolar correlations has been found. While this issue might get fixed at the light of more accurate, forthcoming data, it is important to keep an eye open on different possibilities and explore scenarios able to produce different types of PTA angular correlations. We point out that a stationary non-Gaussian component to the gravitational wave background can modulate the two-point PTA overlap reduction function, adding contributions that can help in fitting the angular distribution of PTA data. We discuss possible sources for such non-Gaussian signal in terms of cosmological processes occurring after inflation ends, and we investigate further tests for this idea.

DOI: 10.1103/PhysRevD.105.083506

I. MOTIVATIONS

Pulsar-timing arrays (PTA) offer a promising tool for detecting gravitational waves (GW) in the nano-Hertz regime. The concept was first proposed in [1–4] and much developed thereafter, see, e.g., [5] for a review. Recently, the NANOGrav Collaboration detected a signal compatible with a stochastic gravitational wave background (SGWB) [6]. Subsequently, the PPTA [7], EPTA [8], and IPTA [9] Collaborations obtained preliminary results going in the same direction. A natural astrophysical source for such a SGWB is constituted by unresolved GW signals from supermassive black hole mergers [10–12]. However, PTA GW detections can also be explained by cosmological sources as GW echoes from primordial black hole formation [13–15], cosmic strings [16–19], phase transitions [20–24], or primordial magnetic field production [25,26]. A puzzling feature of PTA measurements so far is that the constraints on spatial correlations seem to show some deviations from the Hellings-Downs (HD) quadrupolar angular distribution [27], which is a consequence of Einstein general relativity, see, e.g., Fig. 7 in [6] for NANOGrav, Fig. 3 in [7] for PPTA, and Fig. 2 in [8] for EPTA. In case such behavior persists after more data are collected, it will require some departure from the standard approach. A possibility, considered, for example, in [28], is that NANOGrav is detecting extra GW polarizations besides Einstein's spin-2 ones [29,30], since the inclusion of non-Einsteinian polarizations modifies the HD angular distribution [31–34]. A systematic analysis by the NANOGrav Collaboration does not presently favor this option [35], but it recommends one to study this topic further at the light of forthcoming data. In this context, however, we point out that a recent analysis from the LIGO-Virgo-Kagra Collaboration does not provide evidence for non-Einsteinian GW polarizations in the deci-Hertz regime [36].

In this work, motivated from the aforementioned preliminary results of PTA observations, we explore an alternative mechanism for modifying the quadrupolar HD angular distribution, using only the massless spin-2 degrees of freedom of general relativity. We show that large tensor non-Gaussianity can modulate the angular two-point PTA overlap reduction function (ORF) and parametrically change its profile as a function of the angle between pulsars. The non-Gaussianity of the SGWB is an observable not often considered in the GW literature. It has been realized for a long time that, thanks to the central limit theorem, astrophysical SGWB signals are expected to be Gaussian, being the cumulative contribution of many unresolved sources [37]. However, cosmological SGWB sources—inflation, phase transitions, etc.—are coherent and can be characterized by large tensor non-Gaussianity, see, e.g., [38], Sec. V for a review. In general, tensor non-Gaussianity from cosmological sources *cannot* be directly measured with GW experiments, since it leads to nonstationary signals which lose their crucial phase correlations in their way from emission to detection [39–41].[1] A possible way out is to focus on the specific momentum shape corresponding to folded tensor non-Gaussianities, that in real space leads to a stationary signal that does not

[1]Similar effects were previously studied in [42] in the context of two-point functions from inflation. Notice that indirect effects of tensor non-Gaussianities can be detected through correlators of SGWB anisotropies [43–45].

necessarily suffer from the aforementioned problems [46]. Folded non-Gaussianities can arise in scenarios where a stochastic background is generated by *causal* sources [47].[2] In fact, as described in [47], a folded non-Gaussian shape is associated with poles at physical momenta in the connected n-point functions and is a consequence of non-Gaussian cosmological signals produced by mechanisms that preserve locality and causality. Explicit computations of tensor non-Gaussianities from postinflationary cosmological sources are carried out in [48], including scenarios of cosmological phase transitions capable to generate connected n-point correlators ($n > 2$), with an amplitude comparable to the one of two-point correlators. The work [48] focussed on equilateral configurations for n-point functions in momentum space, though without discussing folded configurations that—as argued in [47]—can generally contribute to classical n-point functions in Fourier space.

Our discussion proceeds as follows. In Sec. II, we show how nonlinear effects associated with tensor non-Gaussianity can modulate the angular distribution two-point overlap reduction function. We compute how the resulting ORF profile depends on quantities characterizing the higher-order tensor correlation functions. In the hypothesis that next releases of PTA data will show a significant departure from HD angular correlations, it will be important to design tests to distinguish among different explanations for this phenomenon. For this reason, as a specific prediction of the proposal elaborated in Sec. II, in Sec. III, we analyze four-point connected correlation functions of PTA signals, showing that their detection would indicate the presence of tensor non-Gaussianities in the SGWB. Section IV contains our conclusions, which are followed by four technical Appendixes, elaborating the results presented in the main text.

II. MODULATION OF THE PTA TWO-POINT OVERLAP REDUCTION FUNCTION

In this section, we show that stationary tensor non-Gaussianity can affect the two-point function of PTA signals and parametrically change the angular distribution of the corresponding overlap reduction function (ORF), with respect to the Hellings-Downs (HD) curve. In this work, we take a phenomenological perspective, leaving a more general treatment and a systematic investigation of model building to future studies.

In order to describe a SGWB, we express the GW modes in terms of spin-2 fluctuations around flat space as

$$g_{\mu\nu}dx^\mu dx^\nu = -dt^2 + (\delta_{ij} + h_{ij}(t,\vec{x}))dx^i dx^j, \tag{2.1}$$

with $h_{ij}(t,\vec{x})$ the tensor fluctuation satisfying the transverse-traceless condition $h^i_i = \partial^i h_{ij} = 0$.

The presence of a GW deforms light geodesics and induces a time delay ΔT_α on the period T_α of a pulsar α, located at a position $\vec{x}_\alpha = \tau_\alpha \hat{x}_\alpha$ with respect to the Earth at $\vec{x} = 0$. (We denote τ_α the travel time from source to detection, and we set $c = 1$ from now on.) Denoting with $\hat{n}$ the direction of the GW and introducing the convenient combination

$$E_\alpha(t,\vec{x}) \equiv \hat{x}^i_\alpha \hat{x}^j_\alpha h_{ij}(t,\vec{x}), \tag{2.2}$$

we find the following expression for the time delay z_α induced by the GW:

$$\begin{aligned} z_\alpha \equiv \frac{\Delta T_\alpha(t)}{T_\alpha} = \frac{1}{2(1+\hat{x}_\alpha\cdot\hat{n})}\Big[& E_\alpha(t,\vec{x}=0) - E_\alpha(t-\tau_\alpha,\vec{x}=\vec{x}_\alpha) \\ & -\frac{3}{4}(E^2_\alpha(t,\vec{x}=0) - E^2_\alpha(t-\tau_\alpha,\vec{x}=\vec{x}_\alpha)) \\ & +\frac{5}{16}(E^3_\alpha(t,\vec{x}=0) - E^3_\alpha(t-\tau_\alpha,\vec{x}=\vec{x}_\alpha)) + \ldots\Big]. \end{aligned} \tag{2.3}$$

The first line of Eq. (2.3) is the classic result of [2] (see, e.g., [49], chapter 23, for a textbook derivation). The second and third lines are higher-order corrections associated with nonlinearities in h_{ij} and are a new result of this work. We present in Appendix A a derivation of Eq. (2.3), including a generalization valid for any power in an expansion in E_α.

We proceed analyzing here the two-point correlation functions among pulsar time delays, given by $\langle z_\alpha z_\beta\rangle$ (with α, β denoting the two pulsars). Given the nonlinear structure of Eq. (2.3), we expect that the PTA two-point correlator is modulated by higher-order connected n-point functions involving spin-2 fluctuations h_{ij}. This phenomenon can change the angular dependence of the PTA overlap function.

We expand the transverse-traceless GW gauge in Fourier modes as

$$h_{ij}(t,\vec{x}) = \sum_\lambda \int_{-\infty}^{\infty} df \int d^2\hat{n} e^{-2\pi i f \hat{n}\vec{x}} e^{2\pi i f t} \mathbf{e}^{(\lambda)}_{ij}(\hat{n}) h_\lambda(f,\hat{n}), \tag{2.4}$$

where f is the GW frequency, and the unit vector $\hat{n}$ controls its direction. We formally integrate over positive as well as negative frequencies, and the reality of $h_{ij}(t,\vec{x})$ imposes the condition $h_\lambda(-f,\hat{n}) = h^*_\lambda(f,\hat{n})$ on the Fourier modes. The polarization states for the spin-2 fields are $\lambda = (+,\times)$. Our conventions for the polarization tensors $\mathbf{e}^{(\lambda)}_{ij}(\hat{n})$, and some of their properties, are spelled out in Appendix B.

We assume that the GW spectrum is unpolarized, with a two-point function given by

[2]The work [47] specifically focusses on scalar fluctuations, but its general arguments apply to tensor fluctuations as well (see also Appendix C).

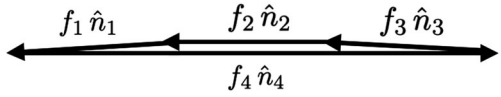

FIG. 1. A folded quadrangle configuration for momenta in Fourier space, satisfying the δ-function conditions of Eq. (2.6). The short sides of the quadrangle are superimposed on the long one.

$$\langle h_{\lambda_1}(f_1,\hat{n}_1)h_{\lambda_2}(f_2,\hat{n}_2)\rangle = \delta_{\lambda_1\lambda_2}\delta(f_1+f_2)\delta^{(2)}(\hat{n}_1-\hat{n}_2)P(f_1), \tag{2.5}$$

where the δ-function conditions are associated with momentum conservation. Additionally, we assume that the SGWB is non-Gaussian, and we parametrize its properties in terms of a nonvanishing four-point function in momentum space,

$$\langle \Pi_{i=1}^4 h_{\lambda_i}(f_i,\hat{n}_i)\rangle = \Pi_{i=1}^3\delta^{(2)}(\hat{n}_4-\hat{n}_i)\delta(f_4+3f_i) \times H_{\lambda_1\ldots\lambda_4}(f_4)P(f_4). \tag{2.6}$$

The non-Gaussian shape associated with Eqs (2.6) corresponds to a folded quadrangle, with three small sides of the quadrangle of equal length and superimposed on the fourth, longest one (see Fig. 1). We focus on the four-point function as [50], being a convenient quantity in treating the modulation effects of the ORF.[3] The condition that the short length sides of the folded quadrangle are equal—as forced by the $\delta(f_4+3f_i)$ conditions in (2.6)—is chosen for simplifying our arguments. The amplitude in (2.6) is proportional to the power spectrum $P(f)$ as introduced in Eq. (2.5). We include as coefficient of Eq. (2.6) a model-dependent tensor $H_{\lambda_1\ldots\lambda_4}(f)$, depending on the polarization indexes and on frequency. A folded tensor non-Gaussianity can arise in scenarios where a cosmological SGWB is produced by cosmological sources after inflation ends. In fact, interactions in such scenarios preserve locality and causality and lead to characteristic poles in higher-order correlation functions which amplify non-Gaussian folded shapes. We refer to Appendix C for additional explanations and an explicit example.

A folded non-Gaussianity in Fourier space leads to a stationary four-point function in real space [46],

$$\langle \Pi_{m=1}^4 h_{i_m j_m}(t_m,\vec{x}_m)\rangle = \sum_{\lambda_i}\int df d^2\hat{n} e^{2\pi i f[(t_1-t_4)+(t_2-t_4)+(t_3-t_4)]} e^{-2\pi i f\hat{n}[(\vec{x}_1-\vec{x}_4)+(\vec{x}_2-\vec{x}_4)+(\vec{x}_3-\vec{x}_4)]} P(f)[H_{\lambda_1\lambda_2\lambda_3\lambda_4}(f)\mathbf{e}^{(\lambda_1)}_{i_1j_1}(\hat{n})\mathbf{e}^{(\lambda_2)}_{i_2j_2}(\hat{n})\mathbf{e}^{(\lambda_3)}_{i_3j_3}(\hat{n})\mathbf{e}^{(\lambda_4)}_{i_4j_4}(\hat{n})], \tag{2.7}$$

which depends on time and on space differences only. As a matter of principle, the stationarity condition in Eq. (2.7) can allow us to circumvent the arguments developed in [39–41], which finds that tensor non-Gaussianity cannot be directly measured with GW experiments. Along their way from source to detection, GW lose their phase correlations due to random effects associated with Shapiro time delays induced by cosmic fluctuations. However, if measurements depend on time differences only—as in the stationary case of Eq. (2.7)—cumulative disturbances cancel out, and the results depend only on the relatively small time differences between successive measurements of pulsar-timing periods. In fact, we can assume that any further (nonfolded) contribution to the four-point function leads to a nonstationary signal which is not directly measurable in terms of correlators of PTA measurements, and we focus on non-Gaussian contributions associated with Eq. (2.6) only, see [46] for more details and [42] for similar considerations for the case of (non)stationary contributions to primordial two-point functions.

[3]In fact, applying the procedure of [50] to the PTA case, one finds that contributions from the three-point function vanish, while the four-point function is able to modulate the ORF, see Appendix B.

As mentioned above, we are assuming that the amplitude of the four-point function in Fourier space, Eq. (2.6), is proportional to the power spectrum $P(f)$ (times the model-dependent function of frequency and polarization indexes, $H_{\lambda_1\ldots\lambda_4}$). Coherent cosmological sources, which are able to amplify the GW spectrum by causal mechanisms, make use of strong nonlinear interactions for the fields involved. They are expected to enhance not only the two-point but also the n-point GW correlation functions with $n>2$; the amplitude of n-point correlators can be of the same order of the two-point one [48]. It would be interesting to study more systematically at what extent these phenomena enhance folded limits of n-point correlation functions, depending on the scenarios considered. We discuss a preliminary example in Appendix C, leaving more detailed analysis to future studies.

The quantity $H_{\lambda_1\ldots\lambda_4}$ describes the dependence of the four-point function on the helicity indexes λ_i. We phenomenologically parametrize it as follows:

$$H_{\lambda_1\lambda_2\lambda_3\lambda_4} \equiv \kappa_1(f)\delta_{\lambda_1\lambda_2}\delta_{\lambda_3\lambda_4} + \kappa_2(f) \times (1-\delta_{\lambda_1\lambda_2})(1-\delta_{\lambda_3\lambda_4})\delta_{\lambda_1\lambda_3}\delta_{\lambda_2\lambda_4}, \tag{2.8}$$

in terms of two frequency-dependent parameters $\kappa_{1,2}(f)$. It is straightforward to consider more general forms for the

tensor $H_{\lambda_1\ldots\lambda_4}$ as a function of the polarization indexes; we explored other choices and found that the previous ansatz describes well the possible angular dependencies of the the-point overlap reduction functions. We stress that our hypotheses are phenomenologically motivated by the aim of making our considerations as transparent as possible. They can be generalized to study more general cases, as indicated by specific model building.

We make use of the results so far for computing the equal-time two-point correlation functions of two pulsar time delays, using formula Eq. (2.3). For the case of a single GW propagating through the direction $\hat{n}$, we find

$$\langle z_\alpha z_\beta\rangle \equiv \left\langle \frac{\Delta T_\alpha}{T_\alpha}\frac{\Delta T_\beta}{T_\beta}\right\rangle = \frac{\langle E_\alpha E_\beta\rangle + 9/16(\langle E_\alpha^2 E_\beta^2\rangle) + 5/4(\langle E_\alpha^3 E_\beta\rangle + \langle E_\alpha E_\beta^3\rangle)}{4(1+\hat{x}_\alpha\cdot\hat{n})(1+\hat{x}_\beta\cdot\hat{n})}, \tag{2.9}$$

where the quantities in this expression are evaluated at the Earth position $E_{\alpha,\beta} = E_{\alpha,\beta}(t,\vec{x}=0)$. The second and third terms in the numerator of Eq. (2.9) are new parts—absent in the Gaussian case—being associated with the higher-order contributions in (2.3). These terms can modulate the overlap reduction functions, as we learn. Contributions of "pulsar terms" of $E_{\alpha,\beta}$ to the two-point functions, which are evaluated at pulsar positions, are uncorrelated with the Earth terms at $\vec{x}=0$. They lead to rapidly oscillating pieces when integrating over frequencies and can be neglected in the present instance as in the standard Gaussian case, see, e.g., the discussion in [49].

We explicitly carry on the calculation of the two-point correlator $\langle z_\alpha z_\beta\rangle$ in Appendix B; the result can be expressed as

$$\langle z_\alpha z_\beta\rangle = \frac{8\pi}{3}\int df P(f)\Gamma_{\alpha\beta}(f). \tag{2.10}$$

The overlap reduction function $\Gamma_{\alpha\beta}(f)$, for the case $\kappa_2 = -4\kappa_1$, results in

$$\Gamma_{\alpha\beta}(f) = \frac{1}{2} - \frac{x_{\alpha\beta}}{4}\left(1-\frac{54}{5}\kappa_1\right) - \frac{171\kappa_1 x_{\alpha\beta}^2}{10} + \frac{72\kappa_1 x_{\alpha\beta}^3}{5} + \frac{3}{2}x_{\alpha\beta}(1-9\kappa_1 x_{\alpha\beta}^2)\ln x_{\alpha\beta}, \tag{2.11}$$

with

$$x_{\alpha\beta} \equiv \frac{1}{2}(1-\cos\zeta_{\alpha\beta}), \tag{2.12}$$

and $\zeta_{\alpha\beta}$ the angle between the two vectors controlling the pulsar positions $\vec{x}_\alpha$, $\vec{x}_\beta$ with respect to the Earth. We understand the dependence on frequency of κ_1, and the more general case of arbitrary $\kappa_{1,2}$ is discussed in Appendix B. Notice that when $\kappa_1 = \kappa_2 = 0$, we recover the standard HD curve. We plot the corresponding two-point ORF in Fig. 2 for some representative choices of constant parameters $\kappa_{1,2}$.

The new ORF profiles shown in Fig. 2 have the tendency to smooth the anticorrelations characterizing the HD curve for angular separations $\zeta_{\alpha\beta} \simeq \pi/2$. This reduction of anti-correlations is a feature in common with other ORF profiles, as the ones induced by a monopole or a scalar contribution, see, e.g., [35]. In the present instance, we refrain from pursuing a proper fit of our parametrization (2.11) with existing PTA data and from performing a dedicated statistical analysis. In fact, current results still have systematic uncertainties (for example, in modeling Solar System ephemeris, as explained in [35]) which will be cured by more accurate, forthcoming data releases. But above all, in our scenario, the time-residual correlators are non-Gaussian; hence, we cannot use the statistical methods based on Gaussian multidimensional likelihoods, see, e.g., [51,52]. We should elaborate a dedicated analysis to the non-Gaussian context we are interested in, also including the frequency dependence for the quantities $\kappa_{1,2}$ appearing in our ORF as motivated by specific models. This goes

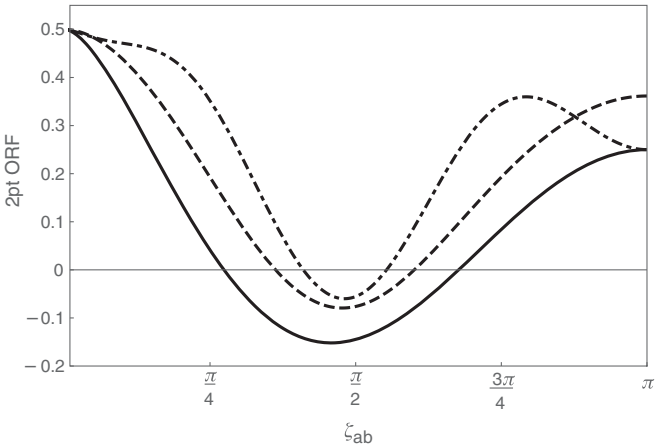

FIG. 2. The PTA two-point overlap reduction function of Eq. (2.10). Solid line: $\kappa_1 = \kappa_2 = 0$ in Eq. (2.11) (HD curve). Dotted-dashed line: $\kappa_1 = 2$, $\kappa_2 = -8$ in Eq. (2.11). Dashed line: $\kappa_1 = 10$, $\kappa_2 = 0$ in Eq. (B13) [we normalize the curve in such a way that its value matches $1/2$ at $\zeta_{\alpha\beta} = 0$; as for the HD curve, see the explanation after Eq. (B13)].

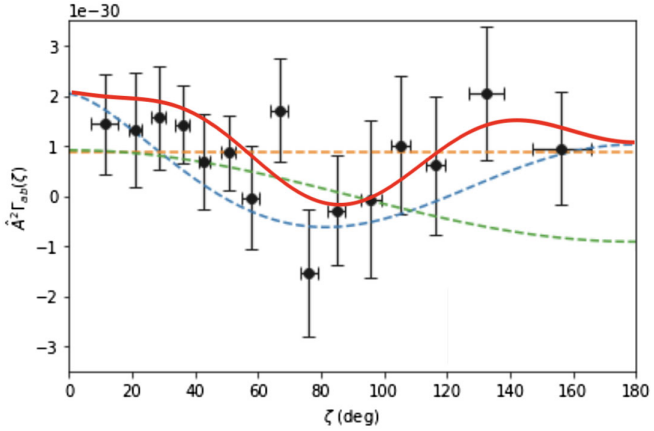

FIG. 3. Visual representation of how the modulated ORF of Eq. (2.11) with $\kappa_1 = 2$, $\kappa_2 = -8$, shown as continuous red line, compares against binned NANOGrav 12.5 data [6]. We include additional ORF profiles, as [6]: dashed blue line, Hellings-Down curve; dashed orange line, monopole ORF; dashed green line, dipole ORF. Figure obtained starting from the content in [57]. To allow for a more direct visual comparison, we use the same conventions and notation of [6] (see their Fig. 5).

beyond the scope of this theoretical work, and we postpone it to future analysis,[4] in the case that forthcoming PTA data will not favor HD-type angular correlations.

Nevertheless, for visual aid only, we represent in Fig. 3 in red color our ORF profile of Eq. (2.11) against binned NANOGrav 12.5 data [6], choosing $\kappa_1 = 2$, $\kappa_2 = -8$. We also include the HD, the monopole, and dipole ORF profiles. This figure is obtained starting from the content in the NANOGrav tutorial website https://data.nanograv.org/, based on [51,54–56], which explains how to obtain Fig. 5 of [6]. Suggestively, the red line corresponding to our ORF apparently fits the data well.

III. A TEST: FOUR-POINT CORRELATON FUNCTIONS OF PTA SIGNALS

In case future PTA data will provide support for a two-point ORF different from the Hellings-Downs curve, it will be crucial to design methods for distinguishing among different explanations for this phenomenon. We propose a smoking gun test for the non-Gaussian mechanism we outlined in the previous section, extending to the PTA case the idea developed in [50] in the context of ground-based GW detectors. We consider the following connected four-point correlation function among PTA time-delay signals[5] $z_{\alpha,\beta}$ induced by GW:

$$\mathcal{K}_{\alpha\beta}(t_1,t_2) \equiv \langle z_\alpha(t_1)z_\alpha(t_2)z_\beta(t_1)z_\beta(t_2)\rangle - \langle z_\alpha(t_1)z_\alpha(t_2)\rangle\langle z_\beta(t_1)z_\beta(t_2)\rangle - \langle z_\alpha(t_1)z_\beta(t_1)\rangle\langle z_\alpha(t_2)z_\beta(t_2)\rangle - \langle z_\alpha(t_1)z_\beta(t_2)\rangle\langle z_\alpha(t_2)z_\beta(t_1)\rangle, \tag{3.1}$$

$$= \frac{8\pi}{3}\int df e^{4\pi i f(t_1-t_2)} P(f) R_{\alpha\beta}(f). \tag{3.2}$$

The combination of the last three terms in Eq. (3.1) is included in order to isolate the connected contribution to the PTA four-point function, depending on the tensor four-point function of Eq. (2.6). In passing from Eq. (3.1) to Eq. (3.2), we make use of Eq. (2.7). The quantity $\mathcal{K}_{\alpha\beta}(t_1,t_2)$ is stationary, since it depends on time differences only. We learn that it is nonvanishing only in the presence of four-point tensor non-Gaussianity, being it proportional to the quantities $\kappa_{1,2}$ entering in the four-point correlator of Eqs. (2.6) and (2.8). We build $\mathcal{K}_{\alpha\beta}(t_1,t_2)$ in terms of signals from two pulsars only, α and β (instead of four distinct pulsars), for handling more easily the expressions involved and for being able to represent the corresponding ORF in terms of a single angle $\zeta_{\alpha\beta}$.

The quantity $R_{\alpha\beta}(f)$ is the PTA four-point ORF and can be expressed in terms of the quantity $x_{\alpha\beta}$ as defined in Eq. (2.12) and of the quantities $\kappa_{1,2}$ which characterize the polarization tensor H_{λ_i} given in Eq. (2.8). We find (see Appendix B),

$$R_{\alpha\beta} = \frac{3}{40}(4\kappa_1+\kappa_2) - \frac{x_{\alpha\beta}}{40}(12\kappa_1 - 137\kappa_2) + \frac{x_{\alpha\beta}^2}{80}(4\kappa_1 - 279\kappa_2) + \frac{3x_{\alpha\beta}\kappa_2}{2}\left(1+\frac{3}{2}x_{\alpha\beta}\right)\ln x_{\alpha\beta}. \tag{3.3}$$

In computing Eq. (3.3), we make use use only of the linear terms in the numerator of Eq. (2.9), and neglect modulations induced by higher-order, non-Gaussian ones [since Eq. (3.3) is already proportional to non-Gaussian contributions].

The corresponding ORF is represented in Fig. 4 for a representative choice of parameters. Notice that, depending on the relative size of $\kappa_{1,2}$, the amplitude of the ORF $R_{\alpha\beta}$ can differ by around 1 order of magnitude for different choices of parameters. In fact, the angular dependence of the four-point ORF is apparently more sensitive to the

[4]See, for example, [53] for interesting attempts to include non-Gaussian statistics in the modeling of uncorrelated noise sources affecting PTA GW detections.

[5]It is also possible to consider four-point functions between four pulsars, but for simplicity, we consider only two pulsars, α and β.

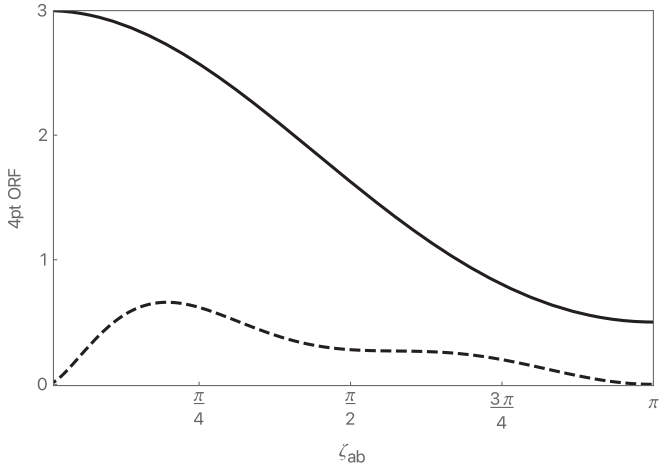

FIG. 4. The PTA four-point overlap reduction function. Solid line: $\kappa_1 = 10$, $\kappa_2 = 0$. Dashed line: $\kappa_1 = 2$, $\kappa_2 = -8$.

helicity structure of the tensor H_{λ_i} with respect to its two-point counterpart of Sec. II. It would then be interesting to consider more general forms of H_{λ_i} than our ansatz of Eq. (2.8) and study their consequences for the four-point ORF.

Let us quantify more the helicity dependence of the four-point PTA overlap functions, with some simple statistical considerations. In Appendix D, we compute the optimal value of the signal-to-noise ratio (SNR) associated with a measurement of the four-point function of Eq. (3.1), as summed over all the available pulsar pairs. We find the general expression

$$\mathrm{SNR}^{\mathrm{opt}} = \sqrt{2T}\left[\frac{1}{S_n^4}\int df |P(f) R_{\mathrm{tot}}(f)|^2\right]^{1/2}, \qquad (3.4)$$

where T is the total duration of measurements, while the pulsar noise S_n is parametrized as in Eq. (D8). R_{tot} is given in Eq. (D10) by the sum of the four-point ORF $R_{\alpha\beta}$ of Eq. (3.3) when evaluated over all distinct pulsar pairs,

$$R_{\mathrm{tot}}(f) = \frac{8\pi}{3}\sum_{\alpha\beta} R_{\alpha\beta}. \qquad (3.5)$$

The quantity R_{tot} can enhance the SNR, if we have several pulsars to sum over; the result will also depend on the specific helicity structure of the quantity H_{λ_i}, in particular, on the values of the parameters $\kappa_{1,2}$ when using ansatz (2.8). For the case of the NANOGrav pulsars, using their angular position that can be extracted from Table 1 of [58], we find the expression

$$R_{\mathrm{tot}}^{\mathrm{NANOGrav}} = 158.5\kappa_1 + 0.2\kappa_2, \qquad (3.6)$$

showing that a NANOGrav measurement of four-point PTA correlations would be more sensitive to the parameter κ_1 with respect to κ_2.

IV. CONCLUSIONS

Several PTA collaborations are finding tantalizing hints for a SGWB signal in the nano-Hertz regime. So far, though, no convincing evidence for Hellings-Downs quadrupolar correlations has been found. While this issue can change at the light of more accurate, forthcoming data, it is meanwhile important to explore scenarios able to produce different types of PTA angular correlations. We pointed out that a stationary non-Gaussian component to the gravitational wave background can modulate the two-point PTA overlap reduction function, modifying its angular dependence with additional parameters that might help in fitting data. We discussed possible sources for such non-Gaussian signals, as well as additional tests of this possibility.

Many questions are left open in order to further elaborate on this idea. It would be interesting to study in detail the shape and amplitude of GW non-Gaussianities in cosmological processes producing a large amplitude of SGWB after inflation ends, since these sources are able to produce the stationary non-Gaussianity we considered in this work. Pursuing a complete analysis in realistic models would be helpful to determine the frequency dependence and helicity structure of the n-point GW correlators that cause the modulation of the PTA overlap functions. In order to perform proper fits with data, it would also be necessary to elaborate on dedicated statistical analysis of signal + noise in the presence of large non-Gaussianities in the signal.

Answering these questions will be interesting and compelling if future PTA data will show evidence for a SGWB but with significant deviations from Hellings-Downs angular correlations.

ACKNOWLEDGMENTS

It is a pleasure to thank Debika Chowdhury, Emanuela Dimastrogiovanni, Matteo Fasiello, and Sachiko Kuroyanagi for discussions. G. T. is partially supported by the STFC Grant No. ST/T000813/1.

APPENDIX A: COMPUTATION OF THE PTA TIME DELAY, INLCUDING NONLINEARITIES

We extend the classic results of [2] for the computation of PTA time delays in the presence of GW, including effects of GW nonlinearities. We express the space-time metric as (we set $c = 1$),

$$ds^2 = -dt^2 + (\delta_{ij} + h_{ij})dx^i dx^j, \qquad (A1)$$

with h_{ij} the tensor fluctuation in transverse-traceless gauge. We compute the time delay in the pulsar period due to the

presence of a GW. We closely follow the textbook discussion of [49], chapter 23, extending it to the more general, nonlinear case we are interested in.

We evaluate the distance covered by photons traveling towards the Earth, starting from pulsar α at spatial position $x^i_\alpha = x_\alpha \hat{x}^i_\alpha$, with $\hat{x}^i_\alpha$ fixed unit vector controlling the pulsar direction. With the Earth at $\vec{x} = 0$, we get the relation

$$dx^2_\alpha = \frac{dt^2}{1 + h_{ij}\hat{x}^i_\alpha \hat{x}^j_\alpha}, \tag{A2}$$

controlling the infinitesimal geometrical distance covered by light during an interval dt in its way from source to detection. For convenience, in what follows, we assemble the combination $h_{ij}\hat{x}^i_\alpha \hat{x}^j_\alpha$ of Eq. (A2) into the quantity

$$E_\alpha \equiv h_{ij}\hat{x}^i_\alpha \hat{x}^j_\alpha, \tag{A3}$$

which depends on time and space. We assume that the GW, controlled by h_{ij}, moves along a null-like geodesics and has a characteristic frequency $\omega_{\rm GW}$ of the order of the inverse of time it takes for light to arrive from source to detection.

Photons emitted at time $t_{\rm em}$ are detected by an observer at time $t_{\rm obs}$ after covering a comoving distance,

$$d_\alpha = \int_{t_{\rm em}}^{t_{\rm obs}} \frac{dt}{[1 + E_\alpha]^{1/2}} \tag{A4}$$

$$= t_{\rm obs} - t_{\rm em} + \int_{t_{\rm em}}^{t_{\rm em}+d_\alpha+\delta t_o} dt' \left\{ \frac{1}{[1+E_\alpha]^{1/2}} - 1 \right\} \times [t', (t_{\rm em} + d_\alpha + \delta t_o - t')\hat{x}_\alpha]. \tag{A5}$$

Within the squared parentheses, we have the coordinate dependence of the integrand function, which is inside the curly brackets. We use the fact that at time t in the interval between $t_{\rm em}$ and $t_{\rm obs}$ photons lie at position $\vec{x}(t) = (t_{\rm obs} - t)\hat{x}_\alpha$. Moreover, since h_{ij} is small, in first approximation, we write $t_{\rm obs} = t_{\rm em} + d_\alpha + \delta t_o$ in the integral, with δt_o a small quantity depending on E_α. In the limit of vanishing h_{ij}, we have $\delta t_o = 0$.

Suppose a second train of photons emitted at a later time $t_{\rm em} + T_\alpha$, with T_α the pulsar period. We can then express the same quantity d_α of Eq. (A4) as

$$d_\alpha = t'_{\rm obs} - t_{\rm em} - T_\alpha + \int_{t_{\rm em}}^{t_{\rm em}+d_\alpha+\delta t'_o} dt' \left\{ \frac{1}{[1 + E_\alpha]^{1/2}} - 1 \right\} \times [t' + T_\alpha, (t_{\rm em} + d_\alpha + \delta t'_o - t')\hat{x}_\alpha], \tag{A6}$$

with $t'_{\rm obs}$ the new time of detection, and $\delta t'_o$ controls the difference, in the limit of small h_{ij}, between $t'_{\rm obs}$ and $t_{\rm em} + d_\alpha$.

Taking the difference between (A6) and (A5), we find

$$t'_{\rm obs} - t_{\rm obs} = T_\alpha + \Delta T_\alpha, \tag{A7}$$

with ΔT_α given by the difference among the integrals appearing in Eqs. (A6) and (A5). We know that the pulsar period is much smaller than the time travel of light from source to detection. This implies that the product $\omega_{\rm GW} T_\alpha$, which enters in the arguments of the time-dependent function E_α in Eq. (A6), is small. We can expand at first order in T_α, finding the following expression for ΔT_α:

$$\Delta T_\alpha = \frac{T_\alpha}{2} \int_{t_{\rm em}}^{t_{\rm em}+d_\alpha+\delta t_o} dt' \left[\frac{\partial_{t'} E_\alpha(t', \vec{x})}{(1 + E_\alpha(t', \vec{x}))^{3/2}} \right]_{\vec{x}=\vec{x}_0(t')}, \tag{A8}$$

with $\vec{x}_0(t) = t_{\rm em} + d_\alpha + \delta t_o - t$.

We assume that E_α can be modeled in terms of a monochromatic plane wave propagating in a null-like geodesics along the $\hat{n}$ direction,

$$E_\alpha(t, \vec{x}) = E_\alpha(\omega_{\rm GW}(t - \hat{n}\,\vec{x})). \tag{A9}$$

We can plug this expression in the integral of Eq. (A8) and compute the time-delay signal as

$$z_\alpha \equiv \frac{\Delta T_\alpha}{T_\alpha}, = -\frac{1}{1 + \hat{x}_\alpha \cdot \hat{n}} \left[\frac{1}{\sqrt{1 + E_\alpha(t, \vec{x} = 0)}} - \frac{1}{\sqrt{1 + E_\alpha(t - \tau_\alpha, \vec{x} = \vec{x}_\alpha)}} \right], \tag{A10}$$

with $\tau_\alpha = t_{\rm em} + d_\alpha + \delta t_o$ the time travel from source to detection. This expression generalizes the classic results of [2] including nonlinearities in E_α. Expanding up to third order in E_α, we obtain Eq. (2.3) in the main text.

APPENDIX B: COMPUTATION OF THE PTA OVERLAP REDUCTION FUNCTIONS

We denote with $\hat{n}$ the GW direction along the spatial coordinates in a Cartesian system as $(\hat{x}, \hat{y}, \hat{z})$. We introduce two unit spatial vectors $\hat{u}$ and $\hat{v}$ orthogonal to $\hat{n}$,

$$\hat{u} = \frac{\hat{n} \times \hat{z}}{|\hat{n} \times \hat{z}|}, \tag{B1}$$

$$\hat{v} = \frac{\hat{n} \times \hat{u}}{|\hat{n} \times \hat{u}|}. \tag{B2}$$

We can also express these quantities in spherical coordinates as

$$\hat{n} = (\sin\theta\cos\phi, \sin\theta\sin\phi, \cos\theta), \tag{B3}$$

$$\hat{u} = (\cos\theta\cos\phi, \cos\theta\sin\phi, -\sin\theta), \tag{B4}$$

$$\hat{v} = (\sin\phi, -\cos\phi, 0). \tag{B5}$$

The symmetric $(+,\times)$ polarization tensors first introduced in Eq. (2.4) are defined as

$$\mathbf{e}^{(+)}_{ij} = u_i u_j - v_i v_j, \tag{B6}$$

$$\mathbf{e}^{(\times)}_{ij} = u_i v_j + v_i u_j, \tag{B7}$$

and satisfy the normalization condition

$$\mathbf{e}^{(\lambda_1)}_{ij}\mathbf{e}^{(\lambda_2)}_{ij} = 2\delta^{\lambda_1\lambda_2}. \tag{B8}$$

The two vectors $\hat{u}$ and $\hat{v}$ introduced in Eqs. (B1) and (B2) are not the only unit vectors orthogonal to $\hat{n}$; more generally, we can rotate $\hat{u}$ and $\hat{v}$ around $\hat{n}$ by an angle ψ,

$$\hat{u}' = \cos\psi\hat{u} + \sin\psi\hat{v}, \tag{B9}$$

$$\hat{v}' = -\sin\psi\hat{u} + \cos\psi\hat{v}. \tag{B10}$$

Observables should not depend on ψ, as in [50], we average over this angle to determine two-point and four-point overlap functions used in the main text.

For computing the two-point function, we introduce the quantities

$$\bar{E}^{(\lambda)}_{\alpha} = \mathbf{e}^{(\lambda)}_{ij}\hat{x}^i_\alpha\hat{x}^j_\alpha. \tag{B11}$$

The pulsar positions are parametrized with $\hat{x}_\alpha = (0,0,1)$, $\hat{x}_\beta = (\cos\zeta_{\alpha\beta}, 0, \sin\zeta_{\alpha\beta})$. The correlators of Eq. (2.10), once integrated over all GW directions, read

$$\langle z_\alpha(t,\vec{x}_\alpha) z_\beta(t,\vec{x}_\beta)\rangle = \frac{8\pi}{3}\int df P(f)\Gamma_{\alpha\beta}(f). \tag{B12}$$

The two-point overlap reduction function is (as explained above, we average over the angle ψ)

$$\begin{aligned}\Gamma_{\alpha\beta}(f) &= \frac{3}{32\pi^2}\sum_{\lambda_i}\int_0^\pi d\psi\int_0^{2\pi}d\phi\int_0^\pi \sin\theta d\theta\frac{1}{(1+\hat{x}_\alpha\cdot\hat{n})}\frac{1}{(1+\hat{x}_\beta\cdot\hat{n})}\\ &\times\left[\delta_{\lambda_1\lambda_2}\bar{E}^{\lambda_1}_\alpha\bar{E}^{\lambda_2}_\beta + H_{\lambda_1\lambda_2\lambda_3\lambda_4}\left(\frac{9}{8}\bar{E}^{\lambda_1}_\alpha\bar{E}^{\lambda_2}_\alpha\bar{E}^{\lambda_3}_\beta\bar{E}^{\lambda_4}_\beta + \frac{5}{4}E^{\lambda_1}_\alpha E^{\lambda_2}_\alpha\bar{E}^{\lambda_3}_\alpha\bar{E}^{\lambda_4}_\beta + (\alpha\leftrightarrow\beta)\right)\right],\\ &= \left(1+\frac{29(\kappa_2+4\kappa_1)}{140}\right)\left[\frac{140+116\kappa_1+29\kappa_2}{280} - \frac{(140+988\kappa_1+625\kappa_2)}{560}x_{\alpha\beta} + \frac{9}{280}(8\kappa_1+135\kappa_2)x^2_{\alpha\beta}\right.\\ &\left. + \frac{(5492\kappa_1-2659\kappa_2)}{1120}x^3_{\alpha\beta} + \frac{5(4\kappa_1+\kappa_2)}{4}x^4_{\alpha\beta} + \frac{3(4\kappa_1+\kappa_2)}{8}x^5_{\alpha\beta} + \frac{3}{2}x_{\alpha\beta}(1-9\kappa_1x^2)\ln x_{\alpha\beta}\right],\end{aligned} \tag{B13}$$

where we used the tensor $H_{\lambda_1\ldots\lambda_4}$ of Eq. (2.8), and $x_{\alpha\beta}$ is defined in Eq. (2.12). When setting $\kappa_1 = \kappa_2 = 0$, we get the standard HD overlap reduction function. For $\kappa_2 + 4\kappa_1 = 0$, we get the function in Eq. (2.11) of the main draft. The angular integral can be done straightforwardly, for example, using the methods of [51]. In this instance, we used the residue theorem approach of [59]. The overall coefficient of Eq. (B13) has been chosen such that the squared parenthesis approaches the value $1/2$ at small values of $\zeta_{\alpha\beta}$, as the HD curve; we plot the part inside the squared parenthesis in Fig. 2. The angular integration along ψ plays an important role in the computation; we checked that only by using tensor four-point functions one gets a nonvanishing result, while using three-point functions one gets zero [50].

A very similar computation can be done for computing the four-point overlap reduction function discussed in Sec. III. This quantity is given by (we sum over repeated indexes)

$$\begin{aligned}R_{\alpha\beta}(f) &= \frac{3}{128\pi^2}\int_0^\pi d\psi\int_0^{2\pi}d\phi\\ &\times\int_0^\pi \sin\theta d\theta\frac{H_{\lambda_1\lambda_2\lambda_3\lambda_4}(f)\bar{E}^{\lambda_1}_\alpha\bar{E}^{\lambda_2}_\alpha\bar{E}^{\lambda_3}_\beta\bar{E}^{\lambda_4}_\beta}{(1+\hat{x}_\alpha\cdot\hat{n})^2(1+\hat{x}_\beta\cdot\hat{n})^2},\end{aligned} \tag{B14}$$

and performing the angular integrations as above we get Eq. (3.3) in the main text. In computing $R_{\alpha\beta}(f)$ as in Eq. (B14), we make use use only of the linear terms in the numerator of Eq. (2.9) and neglect modulations induced by higher-order, non-Gaussian ones.

APPENDIX C: FOLDED TENSOR NON-GAUSSIANITY FROM CASUAL SOURCES

The aim of this Appendix, following [47], is to show through an explicit example that tensor non-Gaussianities from causal, classical sources can have enhanced support in

a folded shape. With "causal sources", we refer to contributions from causal mechanisms active after inflation ends, for example, associated with the decay of particles in their physical, initial state, due to nonlinear interactions that respect locality and causality. As we see, the corresponding n-point functions have poles at physical momenta, enhancing folded non-Gaussian shapes.

The physically more interesting realizations of these considerations are associated with strong GW sources which become active at subhorizon scales after inflation ends, i.e., during radiation and matter domination. In such systems, the aforementioned locality and causality conditions are met. Examples include phase transitions or secondary sources of GWs associated with phenomena of PBH production. But, for ensuring that our arguments are as transparent as possible, we focus in this Appendix on a system in pure de Sitter space and select a specific local interaction for the tensor modes; essentially, we apply the arguments of [47] to the tensor case.

We start with an explicit computation of connected four-point function of tensor modes using as [47] the method of Green functions to then discuss its physical consequences. Besides the usual free quadratic action for spin-2 tensor fluctuations in de Sitter space, we consider a representative local quartic interaction described by the Hamiltonian density,

$$\mathcal{H}_{\rm int} = -\frac{q_0}{4!}\dot{h}_{ij}^4, \tag{C1}$$

with q_0 a constant, and for simplicity, we neglect cubic interactions, since we focus on four-point correlators. The interaction (C1) allows for tensor fluctuations in their physical state to decay (or annihilate) on shell through a nonlinear $1 \leftrightarrow 3$ process, leading—as we see—to a characteristic pole structure in the four-point correlation functions.

To make more direct connection with standard computations of four-point correlation functions in field theory, in this Appendix, we Fourier expand the spin-2 field implementing a slightly different notation with respect to the main text. We work in conformal time, $\partial_t = a^{-1}(\tau)\partial_\tau$, and write

$$h_{ij}(\tau,\vec{x}) = \sum_\lambda \int \frac{d^3k}{(2\pi)^3} e^{i\vec{k}\vec{x}} \mathbf{e}_{ij}^{(\lambda)}(\hat{k}) \tilde{h}_\lambda(\tau,\vec{k}), \tag{C2}$$

where the Fourier mode is decomposed in terms of classical stochastic quantities as

$$\tilde{h}_\lambda(\tau,\vec{k}) = \hat{a}_\lambda^\dagger(\vec{k})\bar{h}_k(\tau) + \hat{a}_\lambda(-\vec{k})\bar{h}_k^*(\tau), \tag{C3}$$

and we denote $\hat{k} \equiv \vec{k}/|\vec{k}|$, and $k \equiv |\vec{k}|$. The stochastic parameters $\hat{a}_\lambda^\dagger$, $\hat{a}_\lambda$ are classical, commuting quantities satisfying the statistical conditions

$$\langle \hat{a}_{\lambda_1}^\dagger(\vec{k}_1)\hat{a}_{\lambda_2}(\vec{k}_2)\rangle = \frac{1}{2}\delta(\vec{k}_1-\vec{k}_2)\delta_{\lambda_1\lambda_2} = \langle \hat{a}_{\lambda_1}(\vec{k}_2)\hat{a}_{\lambda_2}^\dagger(\vec{k}_1)\rangle, \tag{C4}$$

as ensemble averages, see [47]. The solution for the linearized mode function $\bar{h}_{\lambda,k}(\tau)$ in de Sitter space is

$$\bar{h}_k(\tau) = \frac{\Delta_h}{k^{3/2}} e^{ik\tau}(1-ik\tau), \tag{C5}$$

with Δ_h a constant quantity controlling the spin-2 normalization. These results imply that, working at the linearized level, the equal-time spin-2 correlation functions satisfy

$$\langle \tilde{h}_{\lambda_1}^{(1)}(\tau,\vec{k}_1)\tilde{h}_{\lambda_2}^{(1)}(\tau,\vec{k}_2)\rangle = \delta(\vec{k}_1+\vec{k}_2)\delta_{\lambda_1\lambda_2}\frac{\Delta_h^2}{k_1^3}(1+k_1^2\tau^2). \tag{C6}$$

We now proceed including the effects of interactions. We start from the evolution equations for tensor modes including the quartic interaction (C1) (primes denote derivatives along time),

$$h_{ij}'' + 2\mathcal{H}h_{ij}' - \nabla^2 h_{ij} = \frac{q_0}{12a^2}\partial_\tau(\partial_\tau h_{ij})^3. \tag{C7}$$

Using the properties of the polarization tensors, we can rewrite Eq. (C7) in Fourier space as

$$\begin{aligned}\tilde{h}_\lambda''(\tau,\vec{k}) &+ 2\mathcal{H}\tilde{h}_\lambda'(\tau,\vec{k}) + k^2\tilde{h}_\lambda(\tau,\vec{k}) \\ &= \frac{q_0}{24a^2}\partial_\tau\left[\int \frac{d^3q_1}{(2\pi)^3}\frac{d^3q_2}{(2\pi)^3} H_\lambda^{\lambda_a\lambda_b\lambda_c}\tilde{h}_{\lambda_a}'(\tau,\vec{q}_1)\right. \\ &\left.\times \tilde{h}_{\lambda_b}'(\tau,\vec{q}_2)\tilde{h}_{\lambda_c}'(\tau,\vec{k}-\vec{q}_1-\vec{q}_2)\right],\end{aligned} \tag{C8}$$

with

$$H^{\lambda\lambda_a\lambda_b\lambda_c} = \mathbf{e}_{ij}^{(\lambda)}(\hat{k})\mathbf{e}_{im}^{(\lambda_a)}(\hat{q}_1)\mathbf{e}_{mn}^{(\lambda_b)}(\hat{q}_2)\mathbf{e}_{nj}^{(\lambda_c)}(\hat{k}-\hat{q}_1-\hat{q}_2). \tag{C9}$$

Following [47]. we can use the Green function method for studying the effects of classical nonlinearities and how they source connected n-point correlation functions. The Green function $G_k(\tau,\tau')$ relative to the spin-2 evolution Eq. (C7) in pure de Sitter can be expressed as

$$\begin{aligned}G_k(\tau,\tau') = \frac{2\Delta_h^2}{k^3}\{&\sin[k(\tau-\tau')](1+k^2\tau\tau') \\ &- k(\tau-\tau')\cos[k(\tau-\tau')]\}.\end{aligned} \tag{C10}$$

We can decompose the tensor fluctuation in a linear and cubic term in momentum space ($\tilde{h}_\lambda(\tau,\vec{k}) = \tilde{h}_\lambda^{(1)}(\tau,\vec{k}) + \tilde{h}_\lambda^{(3)}(\tau,\vec{k})$). By using the Green function of Eq. (C10), the formal expression for the spin-2 solution at third order is (the sum over repeated indexes is understood)

$$\tilde{h}_\lambda^{(3)}(\tau,\vec{k}) = \frac{q_0}{24}\int d\tau' \frac{d^3q_1}{(2\pi)^3}\frac{d^3q_2}{(2\pi)^3} H_\lambda^{\lambda_a\lambda_b\lambda_c}\partial_{\tau'}G_k(\tau,\tau')\partial_{\tau'}\tilde{h}^{(1)}_{\lambda_a}(\tau',\vec{q}_1)\partial_{\tau'}\tilde{h}^{(1)}_{\lambda_b}(\tau',\vec{q}_2)\partial_{\tau'}\tilde{h}^{(1)}_{\lambda_c}(\tau',\vec{k}-\vec{q}_1-\vec{q}_2). \quad \text{(C11)}$$

This expression can be used to compute the connected part of the equal-time four-point correlation function of $\tilde{h}_\lambda(\tau,\vec{k})$ at leading order in q_0. We find (understanding the equal-time dependence)

$$\begin{aligned}
&\langle\tilde{h}_{\lambda_1}(\vec{k}_1)\tilde{h}_{\lambda_2}(\vec{k}_2)\tilde{h}_{\lambda_3}(\vec{k}_3)\tilde{h}_{\lambda_4}(\vec{k}_4)\rangle \\
&= \frac{q_0}{4}\int d\tau' \frac{d^3q_1}{(2\pi)^3}\frac{d^3q_2}{(2\pi)^3} H^{\lambda_4}_{\lambda_a\lambda_b\lambda_c}(\partial_{\tau'}G_{k_4})\langle\tilde{h}_{\lambda_1}(\vec{k}_1)\tilde{h}_{\lambda_a}(\vec{q}_1)\rangle\langle\tilde{h}_{\lambda_2}(\vec{k}_2)\tilde{h}_{\lambda_b)}(\vec{q}_2)\rangle\langle\tilde{h}_{\lambda_3}(\vec{k}_3)\tilde{h}_{\lambda_c}(\vec{k}_4-\vec{q}_1-\vec{q}_2)\rangle \\
&= \frac{9q_0}{4}\delta(\vec{k}_1+\vec{k}_2+\vec{k}_3+\vec{k}_4)\frac{\Delta_h^8}{k_1k_2k_3k_4}H_{\lambda_4\lambda_1\lambda_2\lambda_3} \\
&\times\left[\frac{1}{(k_1+k_2+k_3+k_4)^5}+\frac{1}{(k_4-k_1-k_2-k_3)^5}+\frac{1}{(k_1+k_2-k_3+k_4)^5}+\frac{1}{(k_2+k_3+k_4-k_1)^5}\right. \\
&\left.+\frac{1}{(k_1+k_3+k_4-k_2)^5}+\frac{1}{(k_3+k_4-k_1-k_2)^5}+\frac{1}{(k_1+k_3-k_4-k_2)^5}+\frac{1}{(k_1+k_4-k_3-k_2)^5}\right]+\text{perms}, \quad \text{(C12)}
\end{aligned}$$

where

$$H_{\lambda_4\lambda_1\lambda_2\lambda_3} = \mathbf{e}^{(\lambda_4)}_{ij}(\hat{k}_4)\mathbf{e}^{(\lambda_1)}_{im}(-\hat{k}_1)\mathbf{e}^{(\lambda_2)}_{mn}(-\hat{k}_2)\mathbf{e}^{(\lambda_3)}_{nj}(-\hat{k}_1-\hat{k}_2-\hat{k}_4). \quad \text{(C13)}$$

The tensor four-point function (C12) contains poles at physical momenta, which enhance a folded shape of tensor non-Gaussianity, corresponding to a quadrangle with superimposed sides in Fourier space. This example shows that classical correlators from causal sources provide the shape of non-Gaussian signals we are after and which can source the effects discussed in Sec. II. Notice that the divergences at the poles can be smoothed by effects as classical dissipation [47]; nevertheless, the corresponding correlation functions have most of their support in folded shapes.

APPENDIX D: THE OPTIMAL SIGNAL-TO-NOISE RATION FOR THE PTA FOUR-POINT FUNCTION

We determine the optimal signal-to-noise ratio (SNR) for estimating the stationary four-point function considered in Sec. III. We generalize the arguments of [46], which uses methods developed in [51,60] and reviewed in [61]. We assume that the time-delay signal s_α measured with pulsar experiments can be separated in a "true" GW signal z_α [as given in Eq. (3.1)] and uncorrelated noise n_α,

$$s_\alpha = z_\alpha + n_\alpha. \quad \text{(D1)}$$

We then integrate the stationary four-point correlator among signals from two pulsars α and β over the temporal duration T of the experiment, and we define the quantity $\mathcal{Y}_{\alpha\beta}$,

$$\mathcal{Y}_{\alpha\beta} = \int_{-T/2}^{T/2} dt_1 dt_2 \mathcal{K}_{\alpha\beta}(t_1,t_2)\mathcal{F}(t_2-t_1), \quad \text{(D2)}$$

where $\mathcal{K}_{\alpha\beta}(t_1,t_2)$, as in Eq. (3.1), is a product of four signals evaluated at two different times, as measured at the Earth,

$$\mathcal{K}_{\alpha\beta}(t_1,t_2) = s_\alpha(t_1)s_\alpha(t_2)s_\beta(t_1)s_\beta(t_2). \quad \text{(D3)}$$

The function $\mathcal{F}$ in Eq. (D2) is a yet-to-be-determined filter function which decays rapidly with increasing the size of its argument $|t_i - t_j|$.

In defining the SNR $= S/N$, the quantity S corresponds to the connected part of the ensemble average value of $\mathcal{Y}_{\alpha\beta}$ in the presence of the GW signal, see Eq. (3.1); the noise N is the root mean square value of $\mathcal{Y}_{\alpha\beta}$ when the signal is absent. We determine the filter function $\mathcal{F}$ that maximizes the corresponding SNR. We Fourier transform (D2), finding

$$\begin{aligned}
\mathcal{Y}_{\alpha\beta} = &\int_{-\infty}^{\infty} df_A df_B df_C \delta_T(f_A+f_C) \\
&\times \delta_T(f_C-f_B)\tilde{\mathcal{F}}(f_C)\tilde{\mathcal{K}}_{\alpha\beta}(f_A,f_B), \quad \text{(D4)}
\end{aligned}$$

and we introduce $\delta_T(f) \equiv \int_{-T}^{T}\exp[2\pi i f t]dt$, a function with the property $\delta_T(0) = T$. Equation (D4) is the starting point for our computations of S and N.

For the signal S, we use the stationary property (3.1) characterizing the connected GW four-point functions, which implies[6]

[6]The factors of $1/2$ in the arguments of the functions are due to the $e^{4\pi i f(t_1-t_2)}$ factor in Eq. (3.1).

$$\tilde{\mathcal{K}}_{\alpha\beta}(f_A, f_B) = \frac{8\pi}{3}\delta(f_A + f_B)P(f_A/2)R_{\alpha\beta}(f_A/2), \quad \text{(D5)}$$

with $R_{\alpha\beta}$ given in Eq. (3.3). Plugging this expression in Eq. (D4), we find that the "signal" contribution is

$$\begin{aligned} S &= \frac{8\pi}{3}\int_{-\infty}^{\infty} df_A df_B df_C \delta_T(f_A + f_C)\delta_T(f_C - f_B) \\ &\quad \times \tilde{\mathcal{F}}(f_C)\delta(f_A + f_B)P(f_A/2)R_{\alpha\beta}(f_A/2) \\ &= \frac{8\pi T}{3}\int_{-\infty}^{\infty} df \tilde{\mathcal{F}}(f)P(f/2)R_{\alpha\beta}(f/2). \end{aligned} \quad \text{(D6)}$$

We now consider the noise part. We assume the noise has a Gaussian distribution, with two-point correlation function,

$$\langle n_\alpha(t_1)n_\beta(t_2)\rangle = S_n\delta(t_1 - t_2)\delta_{\alpha\beta}. \quad \text{(D7)}$$

For simplicity, we assume a common S_n for all pulsars, that as [60] we parametrize as

$$S_n = 2\Delta t\sigma^2, \quad \text{(D8)}$$

with $1/\Delta t$ the typical measurement cadence, and σ^2 the rms of the noise timing. The noise results

$$N^2 = \langle \mathcal{Y}_{\alpha\beta}\mathcal{Y}_{\alpha\beta}\rangle = TS_n^4\int df|\tilde{\mathcal{F}}(f)|^2. \quad \text{(D9)}$$

We can then build the total SNR assembling the results of Eqs. (D6) and (D9), summing over all the pulsar pairs, and denoting for brevity

$$R_{\rm tot}(f) \equiv \frac{8\pi}{3}\sum_{\alpha\beta}R_{\alpha\beta}(f). \quad \text{(D10)}$$

We find

$$\text{SNR} = \sqrt{T}\frac{\int df\tilde{\mathcal{F}}(f)P(f/2)R_{\rm tot}(f/2)}{S_n^2[\int df|\tilde{\mathcal{F}}(f)|^2]^{1/2}}. \quad \text{(D11)}$$

It is easy to determine the filter function $\tilde{\mathcal{F}}$ that maximizes the previous expression. We introduce a positive definite scalar product between two arbitrary quantities $A_i(f)$,

$$[A_1(f), A_2(f)] \equiv \int df A_1(f)A_2^\star(f)S_n^4. \quad \text{(D12)}$$

Then, the SNR of Eq. (D11) can be schematically expressed as

$$\text{SNR} = \sqrt{T}\frac{[\tilde{\mathcal{F}}(f), P(f/2)R_{\rm tot}(f/2)/S_n^4]}{[\tilde{\mathcal{F}}(f), \tilde{\mathcal{F}}(f)]^{1/2}}, \quad \text{(D13)}$$

and it is maximized by choosing an optimal filter function such that

$$\tilde{\mathcal{F}}(f) = P(f/2)R_{\rm tot}(f/2)/S_n^4. \quad \text{(D14)}$$

Plugging this result in Eq. (D11), we find that the optimal SNR results,

$$\text{SNR}^{\rm opt} = \sqrt{2T}\left[\frac{1}{S_n^4}\int df|P(f)R_{\rm tot}(f)|^2\right]^{1/2}. \quad \text{(D15)}$$

The result depends both on the values of the four-point correlation of the GW signal and on the location of pulsars entering in the quantity $R_{\rm tot}$.

[1] M. Sazhin, Opportunities for detecting ultralong gravitational waves, Sov. Astron. **22**, 36 (1978).
[2] S. L. Detweiler, Pulsar timing measurements and the search for gravitational waves, Astrophys. J. **234**, 1100 (1979).
[3] B. Mashhoon, On the detection of gravitational radiation by the doppler tracking of spacecraft, Astrophys. J. **227**, 1019 (1979).
[4] B. Bertotti and B. J. Carr, The prospects of detecting gravitational background radiation by doppler tracking interplantary spacecraft, Astrophys. J. **236**, 1000 (1980).
[5] A. N. Lommen, Pulsar timing arrays: The promise of gravitational wave detection, Rep. Prog. Phys. **78**, 124901 (2015).
[6] Z. Arzoumanian *et al.* (NANOGrav Collaboration), The NANOGrav 12.5 yr Data Set: Search for an isotropic stochastic gravitational-wave background, Astrophys. J. Lett. **905**, L34 (2020).
[7] B. Goncharov *et al.*, On the evidence for a common-spectrum process in the search for the nanohertz gravitational-wave background with the Parkes pulsar timing array, Astrophys. J. Lett. **917**, L19 (2021).
[8] S. Chen *et al.*, Common-red-signal analysis with 24-yr high-precision timing of the European Pulsar Timing Array: Inferences in the stochastic gravitational-wave background search, Mon. Not. R. Astron. Soc. **508**, 4970 (2021).
[9] J. Antoniadis *et al.*, The international pulsar timing array second data release: Search for an isotropic gravitational wave background, Mon. Not. R. Astron. Soc. **510**, 4873 (2022).

[10] M. G. Haehnelt, Low frequency gravitational waves from supermassive black holes, Mon. Not. R. Astron. Soc. **269**, 199 (1994).
[11] A. Sesana, F. Haardt, P. Madau, and M. Volonteri, Low—frequency gravitational radiation from coalescing massive black hole binaries in hierarchical cosmologies, Astrophys. J. **611**, 623 (2004).
[12] A. Sesana, A. Vecchio, and C. N. Colacino, The stochastic gravitational-wave background from massive black hole binary systems: Implications for observations with Pulsar Timing Arrays, Mon. Not. R. Astron. Soc. **390**, 192 (2008).
[13] V. Vaskonen and H. Veermäe, Did NANOGrav See a Signal from Primordial Black Hole Formation?, Phys. Rev. Lett. **126**, 051303 (2021).
[14] V. De Luca, G. Franciolini, and A. Riotto, NANOGrav Data Hints at Primordial Black Holes as Dark Matter, Phys. Rev. Lett. **126**, 041303 (2021).
[15] K. Kohri and T. Terada, Solar-mass primordial black holes explain NANOGrav hint of gravitational waves, Phys. Lett. B **813**, 136040 (2021).
[16] J. Ellis and M. Lewicki, Cosmic String Interpretation of NANOGrav Pulsar Timing Data, Phys. Rev. Lett. **126**, 041304 (2021).
[17] W. Buchmuller, V. Domcke, and K. Schmitz, From NANOGrav to LIGO with metastable cosmic strings, Phys. Lett. B **811**, 135914 (2020).
[18] S. Blasi, V. Brdar, and K. Schmitz, Has NANOGrav Found First Evidence for Cosmic Strings?, Phys. Rev. Lett. **126**, 041305 (2021).
[19] J. J. Blanco-Pillado, K. D. Olum, and J. M. Wachter, Comparison of cosmic string and superstring models to NANOGrav 12.5-year results, Phys. Rev. D **103**, 103512 (2021).
[20] Y. Nakai, M. Suzuki, F. Takahashi, and M. Yamada, Gravitational waves and dark radiation from dark phase transition: Connecting NANOGrav pulsar timing data and hubble tension, Phys. Lett. B **816**, 136238 (2021).
[21] W. Ratzinger and P. Schwaller, Whispers from the dark side: Confronting light new physics with NANOGrav data, SciPost Phys. **10**, 047 (2021).
[22] A. Addazi, Y.-F. Cai, Q. Gan, A. Marciano, and K. Zeng, NANOGrav results and dark first order phase transitions, Sci. China Phys. Mech. Astron. **64**, 290411 (2021).
[23] Z. Arzoumanian *et al.* (NANOGrav Collaboration), Searching for Gravitational Waves from Cosmological Phase Transitions with the NANOGrav 12.5-Year Dataset, Phys. Rev. Lett. **127**, 251302 (2021).
[24] A. Brandenburg, E. Clarke, Y. He, and T. Kahniashvili, Can we observe the QCD phase transition-generated gravitational waves through pulsar timing arrays?, Phys. Rev. D **104**, 043513 (2021).
[25] A. Neronov, A. Roper Pol, C. Caprini, and D. Semikoz, NANOGrav signal from magnetohydrodynamic turbulence at the QCD phase transition in the early Universe, Phys. Rev. D **103**, L041302 (2021).
[26] A. Roper Pol, C. Caprini, A. Neronov, and D. Semikoz, The gravitational wave signal from primordial magnetic fields in the Pulsar Timing Array frequency band, arXiv:2201.05630.
[27] R. w. Hellings and G. s. Downs, Upper limits on the isotropic gravitational radiation background from pulsar timing analysis, Astrophys. J. Lett. **265**, L39 (1983).
[28] Z.-C. Chen, C. Yuan, and Q.-G. Huang, Non-tensorial gravitational wave background in NANOGrav 12.5-year data set, Sci. China Phys. Mech. Astron. **64**, 120412 (2021).
[29] D. M. Eardley, D. L. Lee, and A. P. Lightman, Gravitational-wave observations as a tool for testing relativistic gravity, Phys. Rev. D **8**, 3308 (1973).
[30] D. M. Eardley, D. L. Lee, A. P. Lightman, R. V. Wagoner, and C. M. Will, Gravitational-Wave Observations as a Tool for Testing Relativistic Gravity, Phys. Rev. Lett. **30**, 884 (1973).
[31] S. J. Chamberlin and X. Siemens, Stochastic backgrounds in alternative theories of gravity: Overlap reduction functions for pulsar timing arrays, Phys. Rev. D **85**, 082001 (2012).
[32] J. R. Gair, J. D. Romano, and S. R. Taylor, Mapping gravitational-wave backgrounds of arbitrary polarisation using pulsar timing arrays, Phys. Rev. D **92**, 102003 (2015).
[33] N. J. Cornish, L. O'Beirne, S. R. Taylor, and N. Yunes, Constraining Alternative Theories of Gravity using Pulsar Timing Arrays, Phys. Rev. Lett. **120**, 181101 (2018).
[34] J. D. Romano and N. J. Cornish, Detection methods for stochastic gravitational-wave backgrounds: A unified treatment, Living Rev. Relativity **20**, 2 (2017).
[35] Z. Arzoumanian *et al.* (NANOGrav Collaboration), The NANOGrav 12.5-year data set: Search for non-Einsteinian polarization modes in the gravitational-wave background, Astrophys. J. Lett. **923**, L22 (2021).
[36] R. Abbott *et al.* (LIGO Scientific, Virgo, KAGRA Collaborations), Tests of general relativity with GWTC-3, arXiv:2112.06861.
[37] B. Allen, Stochastic gravity-wave background in inflationary-universe models, Phys. Rev. D **37**, 2078 (1988).
[38] N. Bartolo, V. Domcke, D. G. Figueroa, J. García-Bellido, M. Peloso, M. Pieroni, A. Ricciardone, M. Sakellariadou, L. Sorbo, and G. Tasinato, Probing non-Gaussian stochastic gravitational wave backgrounds with LISA, J. Cosmol. Astropart. Phys. 11 (2018) 034.
[39] N. Bartolo, V. De Luca, G. Franciolini, A. Lewis, M. Peloso, and A. Riotto, Primordial Black Hole Dark Matter: LISA Serendipity, Phys. Rev. Lett. **122**, 211301 (2019).
[40] N. Bartolo, V. De Luca, G. Franciolini, M. Peloso, D. Racco, and A. Riotto, Testing primordial black holes as dark matter with LISA, Phys. Rev. D **99**, 103521 (2019).
[41] A. Margalit, C. R. Contaldi, and M. Pieroni, Phase decoherence of gravitational wave backgrounds, Phys. Rev. D **102**, 083506 (2020).
[42] B. Allen, E. E. Flanagan, and M. A. Papa, Is the squeezing of relic gravitational waves produced by inflation detectable?, Phys. Rev. D **61**, 024024 (1999).
[43] N. Bartolo, D. Bertacca, S. Matarrese, M. Peloso, A. Ricciardone, A. Riotto, and G. Tasinato, Anisotropies and non-Gaussianity of the cosmological gravitational wave background, Phys. Rev. D **100**, 121501 (2019).
[44] N. Bartolo, D. Bertacca, S. Matarrese, M. Peloso, A. Ricciardone, A. Riotto, and G. Tasinato, Characterizing the cosmological gravitational wave background: Anisotropies and non-Gaussianity, Phys. Rev. D **102**, 023527 (2020).
[45] E. Dimastrogiovanni, M. Fasiello, and G. Tasinato, Searching for Fossil Fields in the Gravity Sector, Phys. Rev. Lett. **124**, 061302 (2020).

[46] C. Powell and G. Tasinato, Probing a stationary non-Gaussian background of stochastic gravitational waves with pulsar timing arrays, J. Cosmol. Astropart. Phys. 01 (2020) 017.
[47] D. Green and R. A. Porto, Signals of a Quantum Universe, Phys. Rev. Lett. **124**, 251302 (2020).
[48] P. Adshead and E. A. Lim, 3-pt statistics of cosmological stochastic gravitational waves, Phys. Rev. D **82**, 024023 (2010).
[49] M. Maggiore, *Gravitational Waves. Vol. 2: Astrophysics and Cosmology* (Oxford University Press, New York, 2018), p. 3.
[50] N. Seto, Non-Gaussianity analysis of GW background made by short-duration burst signals, Phys. Rev. D **80**, 043003 (2009).
[51] M. Anholm, S. Ballmer, J. D. E. Creighton, L. R. Price, and X. Siemens, Optimal strategies for gravitational wave stochastic background searches in pulsar timing data, Phys. Rev. D **79**, 084030 (2009).
[52] R. van Haasteren, Y. Levin, P. McDonald, and T. Lu, On measuring the gravitational-wave background using Pulsar Timing Arrays, Mon. Not. R. Astron. Soc. **395**, 1005 (2009).
[53] L. Lentati, M. P. Hobson, and P. Alexander, Bayesian estimation of non-Gaussianity in Pulsar Timing Analysis, Mon. Not. R. Astron. Soc. **444**, 3863 (2014).
[54] P. B. Demorest *et al.*, Limits on the stochastic gravitational wave background from the North American nanohertz observatory for gravitational waves, Astrophys. J. **762**, 94 (2013).
[55] S. J. Chamberlin, J. D. E. Creighton, X. Siemens, P. Demorest, J. Ellis, L. R. Price, and J. D. Romano, Time-domain implementation of the optimal cross-correlation statistic for stochastic gravitational-wave background searches in Pulsar Timing Data, Phys. Rev. D **91**, 044048 (2015).
[56] S. J. Vigeland, K. Islo, S. R. Taylor, and J. A. Ellis, Noise-marginalized optimal statistic: A robust hybrid frequentist-Bayesian statistic for the stochastic gravitational-wave background in pulsar timing arrays, Phys. Rev. D **98**, 044003 (2018).
[57] https://data.nanograv.org/.
[58] Z. Arzoumanian *et al.* (NANOGrav Collaboration), The NANOGrav 11-year Data Set: High-precision timing of 45 Millisecond Pulsars, Astrophys. J. Suppl. Ser. **235**, 37 (2018).
[59] F. A. Jenet and J. D. Romano, Understanding the gravitational-wave Hellings and Downs curve for pulsar timing arrays in terms of sound and electromagnetic waves, Am. J. Phys. **83**, 635 (2015).
[60] E. Thrane and J. D. Romano, Sensitivity curves for searches for gravitational-wave backgrounds, Phys. Rev. D **88**, 124032 (2013).
[61] M. Maggiore, *Gravitational Waves. Vol. 1: Theory and Experiments* Oxford Master Series in Physics (Oxford University Press, New York, 2007).